ISSN (Print) 1598-5385
ISSN (Online) 2233-6648
≪연구논문≫ Journal of the Korean Magnetics Society 35(6), 300-305 (2025) https://doi.org/10.4283/JKMS.2025.35.6.300

Quantification of Large Dzyaloshinskii-Moriya Interaction under Weak Magnetic Fields

Minhwan Kim[1,2] and Duck-Ho Kim[1]*

[1]*Center for Spintronics, Korea Institute of Science and Technology (KIST), Seoul 02792, Republic of Korea*
[2]*Department of Physics and Astronomy, Seoul National University, Seoul 08826, Republic of Korea*

(Received 4 November 2025, Received in final form 19 November 2025, Accepted 20 November 2025)

We introduce a theoretical method for determining large Dzyaloshinskii-Moriya interaction (DMI) values within a specific range of external magnetic fields. Based on the domain-wall (DW) energy model, we establish that, under the low-field approximation, the azimuthal angle of magnetization within the DW-regions where magnetization changes-exhibits a quadratic dependence on the in-plane magnetic field. The corresponding curvature coefficient depends solely on the DMI and DW anisotropy energy. This method can also be used to measure the in-plane field dependence of the normalized damping-like torque efficiency, which represents the DW magnetization for fields normal to the DW. This framework enables reliable quantification of a broad range of DMI magnitudes, overcoming the limitations imposed by the weak magnetic fields typically accessible in experiments.

Keywords : Domain wall, Néel domain wall, Dzyaloshinskii-Moriya interaction (DMI)

저자기장 영역에서 거대 드쟐로신스키 모리아 상호작용 측정법

김민환[1,2] · 김덕호[1]*

[1]한국과학기술연구원 스핀융합연구단, 서울시 성북구 화랑로 14길5, 02792
[2]서울대학교 물리천분학부, 서울시 관악구 관악로1, 08826

(2025년 11월 4일 받음, 2025년 11월 19일 최종수정본 받음, 2025년 11월 20일 게재확정)

본 연구에서는 매우 작은 범위의 외부 자기장에서도 큰 드쟐로신스키–모리아 상호작용(Dzyaloshinskii-Moriya interaction, DMI)을 정밀하게 측정할 수 있는 새로운 이론적 방법을 제시하였다. 자구벽 에너지 모델을 기반으로, 작은 외부 자기장이 인가될 경우 자구벽 내부의 자화가 미세한 각도로 기울어지며, 이때 자구벽 자화의 방위각은 외부 자기장에 대해 2차 함수적으로 변화함을 보였다. 이 2차 항의 곡률 계수는 DMI와 자구벽 이방성 에너지에만 의존함을 확인하였다. 이러한 개념은 자구벽에 수직한 평면 방향으로 인가된 자기장에 따른 스핀궤도토크 효율 측정을 통해 실험적으로 검증할 수 있으며, 이를 통해 큰 DMI 값을 효과적으로 산출할 수 있다. 제안된 이 이론적 틀은 실험적으로 접근 가능한 약한 자기장 범위 내에서도 DMI를 안정적으로 규명할 수 있어, 기존 측정법의 한계를 극복하고 넓은 DMI 세기 범위에 적용 가능한 새로운 측정기법을 제공하였다.

주제어 : 자구벽, 넬 자구벽, 드쟐로신스키 모리아 상호작용

I. Introduction

The Dzyaloshinskii-Moriya interaction (DMI), an antisymmetric exchange interaction [1-4], plays a central role in stabilizing chiral spin textures in magnetic systems [5-11]. Numerous theoretical frameworks have been proposed for understanding the microscopic origin of DMI, while extensive experimental efforts have focused on

*Corresponding author: Tel: +82-2-958-5781, e-mail: uzes@kist.re.kr

tuning its magnitude to achieve large values [12-22]. Various techniques have been developed to quantify the DMI, including spin-wave spectroscopy [17-19], asymmetric domain-wall (DW) motion [12,16,22], domain-edge tilting [14,20], electric detection of spin-wave propagation [21], asymmetric hysteresis-loop analysis [23-25], and spin-orbit-torque (SOT) efficiency measurements based on DW chiral transitions [26,27]. These approaches have enabled a deeper understanding of chiral spin configurations and have fostered diverse studies on current-driven magnetization control through SOT.

Among existing methods, DW-based techniques are particularly advantageous in ferromagnet with perpendicular magnetic anisotropy, as they enable simultaneous evaluation of the spin Hall angle through the SOT efficiency and the DMI [12,16,22-29]. Both parameters are essential for stabilizing chiral spin textures and achieving efficient magnetization control. Conventional DW-based methods require the application of strong in-plane magnetic fields to determine high-strength DMI, demanding experimental facilities that are not readily accessible to most laboratories. Consequently, a method capable of determining large DMI strengths under experimentally limited field ranges is required. We propose a theoretical framework that enables the reliable quantification of large DMI strengths using a conservative range of external magnetic fields. This approach effectively addresses the limitations of conventional methods that require high-field measurements for DMI determination.

II. Result and Discussion

The theoretical framework for DW energetics in systems with DMI originally proposed by Thiaville *et al.* [30] is the foundation of the proposed model. In perpendicularly magnetized materials with finite DMI, the DW naturally adopts a Néel-type DW configuration, where the magnetization within the domain wall aligns along the direction normal to the wall plane, as illustrated in Fig. 1(a). When an in-plane magnetic field is applied perpendicular to the DW plane (defined here as the y-axis field, $\mu_0 H_y$), the magnetization within the DW progressively rotates from the Néel toward the Bloch configuration. Under these conditions, the DW energy $\sigma_{DW}(\mu_0 H_y)$ can be expressed as follows:

$$\sigma_{DW}(\mu_0 H_y) = \sigma_0 + \pi\lambda K_D \cos^2\psi - \pi\lambda M_S \mu_0 H_{DMI} \cos\psi - \pi\lambda M_S \mu_0 H_y \sin\psi, \quad (1)$$

where σ_0 denotes a Bloch-type-DW energy density, K_D represents the DW anisotropy energy density, λ is the DW width, M_S is the saturation magnetization, and $\mu_0 H_{DMI}$ corresponds to the effective magnetic field arising from the DMI. The angle ψ defines the azimuthal orientation of the magnetization within the wall, measured from the +x axis (see the Fig. 1(b) for illustration).

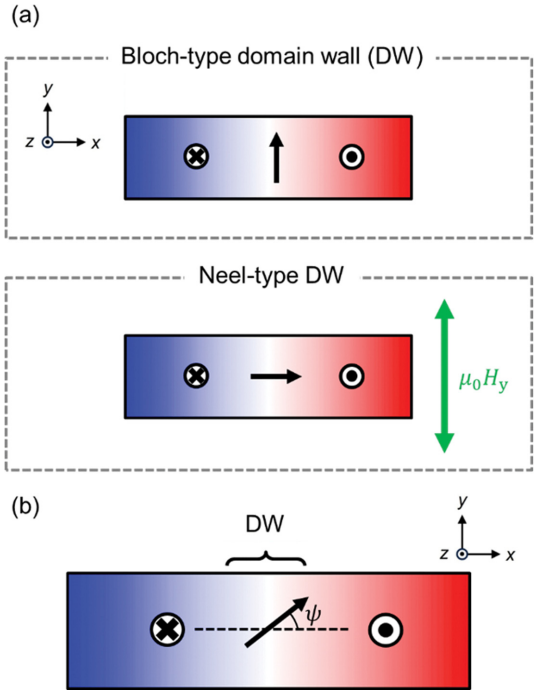

Fig. 1. (Color online) (a) Illustration of the Bloch-type and Néel-type domain walls (DWs). The black arrow indicates the magnetization at DW. The in-plane magnetic field $\mu_0 H_y$ is applied along the DW plane (y-axis). (b) The DW angle ψ defines the azimuthal orientation of the magnetization within the wall, measured from the +x axis.

The equilibrium condition of the azimuthal DW angle can be obtained by minimizing the DW energy with respect to ψ (i.e., $\partial\sigma_{DW}/\partial\psi = 0$) as follows: $-2\pi\lambda K_D \cos\psi_{eq} \sin\psi_{eq} + \pi\lambda M_S \mu_0 H_{DMI} \sin\psi_{eq} - \pi\lambda M_S \mu_0 H_y \cos\psi_{eq} = 0$. Here, ψ_{eq} denotes the equilibrium magnetization angle within the DW. When the applied y-axis magnetic field $\mu_0 H_y$ is sufficiently small such that ψ_{eq} remains within the small-angle regime, the relation $\psi_{eq} \cong \mu_0 H_y / (\mu_0 H_{DMI} - \mu_0 H_S)$ can be derived. A detailed discussion of the small-angle regime, including its theoretical consideration, is provided below in the context of Fig. 2. The DW anisotropy field $\mu_0 H_S$ is defined through the relation $K_D \equiv M_S \mu_0 H_S/2$ [12,30,31]. The following relationship can be derived by substituting the approximated ψ_{eq} into Eq. (1):

$$\sigma_{DW}(\mu_0 H_y) \cong \sigma_0 + \pi\lambda K_D - \pi\lambda M_S \mu_0 H_{DMI} - \frac{\pi\lambda M_S}{2(\mu_0 H_{DMI} - \mu_0 H_S)} \mu_0 H_y^2. \quad (2)$$

Here, $\sigma_{DW}(\mu_0 H_y)$ indicates a quadratic dependence on

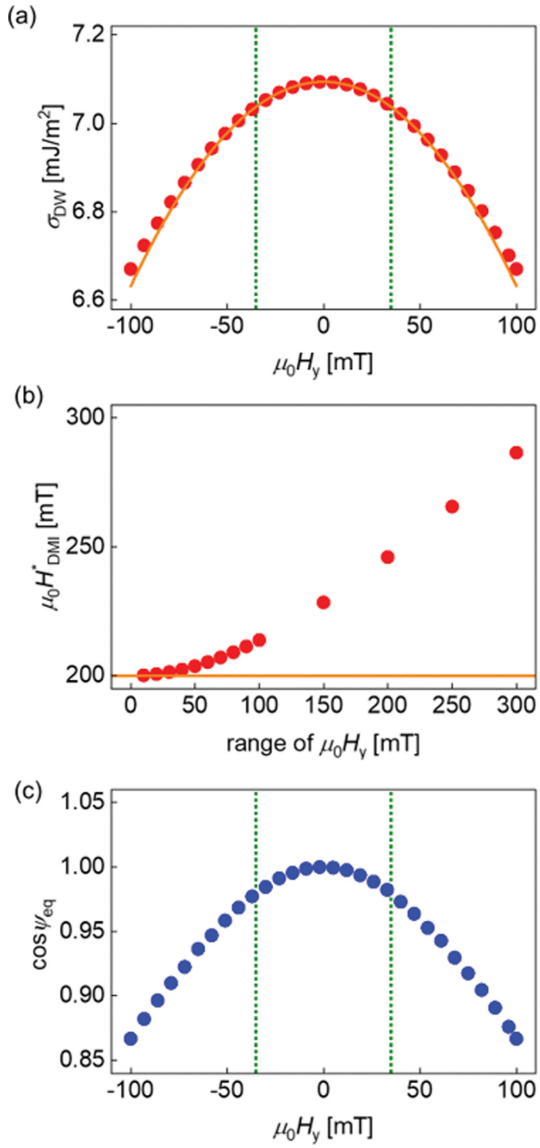

Fig. 2. (a) (Color online) σ_{DW} on $\mu_0 H_y$ under the given conditions: σ_0 = 10 mJ/m^2, $\mu_0 H_S$ = 30 mT, λ = 5 nm, M_S = 1 MA/m, and $\mu_0 H_{DMI}$ = 200 mT (red symbols represent the numerical calculations). The orange solid line is calculated σ_{DW} on $\mu_0 H_y$ using Eq. (2). Green dashed lines are $\mu_0 H_y \cong \pm 35$ mT. (b) $\mu_0 H^*_{DMI}$ as a function of the applied in-plane field range $\mu_0 H_y$ used in the $\sigma_{DW}(\mu_0 H_y)$ analysis based on Eq. (2). The orange solid line is $\mu_0 H_{DMI}$ = 200 mT. (c) Equilibrium magnetization component $\cos\psi_{eq}$ as a function of $\mu_0 H_y$. Green dashed lines are $\mu_0 H_y$ = 35 mT.

$\mu_0 H_y$ in Eq. (2). Furthermore, the curvature coefficient is composed of four physical parameters: $\mu_0 H_{DMI}$, $\mu_0 H_S$, λ, and M_S.

To evaluate the accuracy and determine the applicable range of our analytical approximation, we performed numerical calculations using the exact equilibrium solution of Eq. (1), validating the approximation. The material parameters employed in the analysis were σ_0 = 10 mJ/m^2, $\mu_0 H_S$ = 30 mT, λ = 5 nm, MS = 1 MA/m, and $\mu_0 H_{DMI}$ = 200 mT [12,14,16]. Fig. 2(a) illustrates the dependence of σ_{DW} on $\mu_0 H_y$ under the given conditions (red symbols represent the numerical calculations). As $\mu_0 H_y$ increases, σ_{DW} decreases owing to the Zeeman effect, which lowers the overall DW energy. Using Eq. (2), the corresponding approximated results were obtained numerically (orange solid line in Fig. 2(a)). A noticeable deviation appears beyond $\mu_0 H_y \cong \pm 35$ mT (green dashed lines in Fig. 2(a)), a deviation starts to increase, indicating the out of the approximation as ψ_{eq} exceeds the small-angle regime.

We defined $\mu_0 H^*_y$ as the critical in-plane field at which the small-angle approximation ceases to hold. From Eq. (2), $\mu_0 H_{DMI}$ can be extracted by analyzing the curvature $\kappa = \pi\lambda M_S/2(\mu_0 H_{DMI} - \mu_0 H_S)$ for given values of given λ, M_S, and $\mu_0 H_S$. Accordingly, once κ is determined, the corresponding DMI-induced effective field, denoted as $\mu_0 H^*_{DMI}$, can be defined based on the curvature analysis. The characteristic field $\mu_0 H^*_y$ thus defines the physical limit within which β analysis remains valid.

Fig. 2(b) presents $\mu_0 H^*_{DMI}$ as a function of the applied in-plane field range $\mu_0 H_y$ used in the $\sigma_{DW}(\mu_0 H_y)$ analysis based on Eq. (2). Within a narrow $\mu_0 H_y$ window, $\mu_0 H^*_{DMI}$ agrees well with the intrinsic $\mu_0 H_{DMI}$ (orange solid line). We define $\mu_0 H^*_y$ as the maximum in-plane field range for which the deviation between $\mu_0 H^*_{DMI}$ and $\mu_0 H_{DMI}$ remains within 1%; in Fig. 2(a), this corresponds to $\mu_0 H^*_y \cong 35$ mT. To substantiate this definition, Fig. 2(c) shows the equilibrium magnetization component $\cos\psi_{eq}$ as a function of $\mu_0 H_y$. At $\mu_0 H_y$ = ±35 mT (green dashed lines), $\cos\psi_{eq}$ decreases to about 0.98, indicating a 2% tilt of the magnetization and signaling the breakdown of the small-angle approximation.

We examined the factors governing the magnitude of $\mu_0 H^*_y$ by systematically varying $\mu_0 H_{DMI}$ and $\mu_0 H_S$. Figs. 3(a) and 3(b) display $\mu_0 H^*_y$ as a function of $\mu_0 H_{DMI}$ (for a fixed $\mu_0 H^*_y$ = 30 mT) and as a function of $\mu_0 H_S$ (for a fixed $\mu_0 H_{DMI}$ = 50 mT), respectively. The calculations were performed using σ_0 = 10 mJ/m^2, $\mu_0 H_S$ = 30 mT, λ = 5 nm and M_S = 1 MA/m. As evident from the results, once $\mu_0 H_{DMI}$ exceeds $\mu_0 H_S$, $\mu_0 H_{DMI}$ has predominantly influenced on $\mu_0 H^*_y$, whereas the influence of $\mu_0 H_S$ becomes negligible effect on $\mu_0 H^*_y$. Thus, a larger $\mu_0 H_{DMI}$ emerges as the principal parameter setting the validity limit of the small-angle approximation.

In the following text, we introduce a new approach for measuring the DMI and its corresponding effective field $\mu_0 H_{DMI}$, within the range of in-plane magnetic fields $\mu_0 H_y < \mu_0 H^*_y$, where the small-angle approximation is

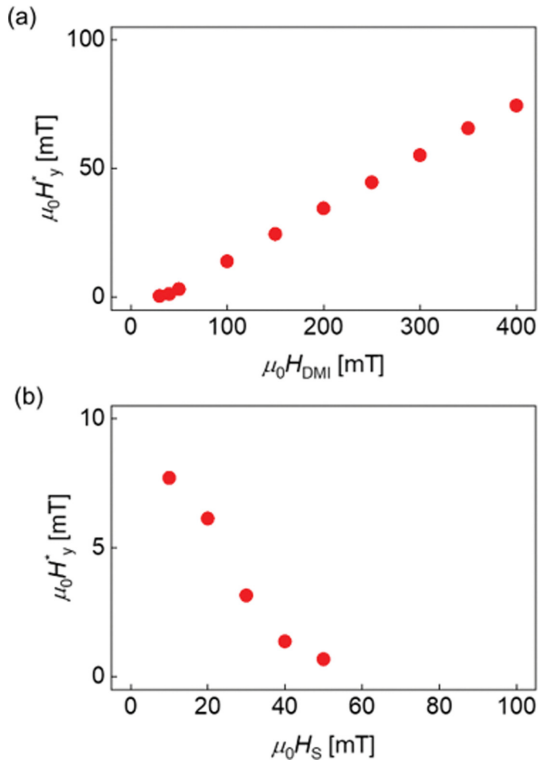

Fig. 3. (Color online) (a) $\mu_0 H^*_y$ as a function of $\mu_0 H_{DMI}$ (for a fixed $\mu_0 H_S$ = 30 mT). (b) $\mu_0 H^*_y$ as a function of $\mu_0 H_S$ (for a fixed $\mu_0 H_{DMI}$ = 50 mT). The calculations were performed using σ_0 = 10 mJ/m^2, $\mu_0 H_S$ = 30 mT, λ = 5 nm and M_S = 1 MA/m.

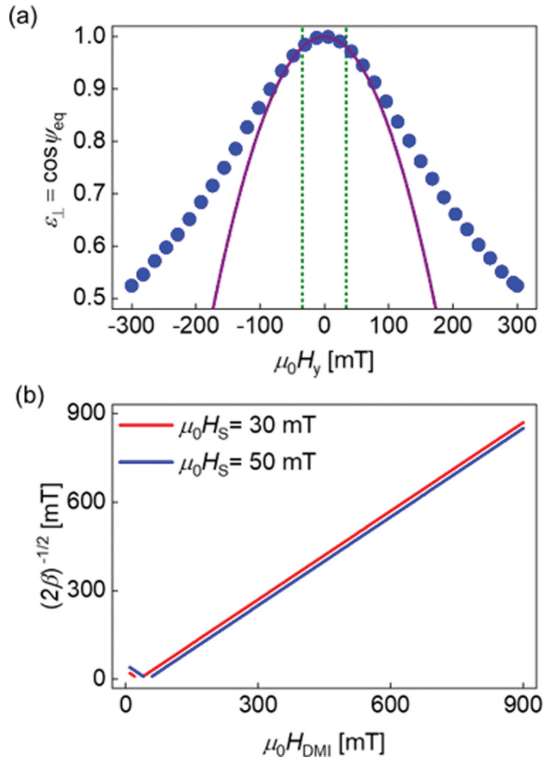

Fig. 4. (Color online) (a) $\varepsilon_\perp$ as a function of $\mu_0 H_y$, where $\varepsilon_\perp = \cos\psi_{eq}$. The material parameters employed in the analysis were σ_0 = 10 mJ/m^2, $\mu_0 H_S$ = 30 mT, λ = 5 nm, M_S = 1 MA/m, and $\mu_0 H_{DMI}$ = 200 mT. The purple solid line represents the calculated values obtained from Eq. (3). (b) $1/\sqrt{2\beta}$ as a function of $\mu_0 H_{DMI}$ for each $\mu_0 H_S$.

valid. Previous studies have demonstrated that $\cos\psi_{eq}$ could be experimentally extracted from SOT-driven DW motion or from the asymmetric hysteresis loop [23-27], where the SOT efficiency ε is given by $\varepsilon = \varepsilon_{sat}\cos\psi_{eq}$. Here, ε_{sat} represents the maximum SOT efficiency for a Néel-type DW, defined as $\varepsilon_{sat} = (\hbar/2e)(\theta/M_S t)$, with $\hbar$ being the reduced Planck constant, e the electron charge, θ the effective Hall angle, and t the ferromagnetic layer thickness. The normalized efficiency $\varepsilon_\perp$ is defined as $\varepsilon_\perp = \cos\psi_{eq}$.

For small in-plane magnetic fields $\mu_0 H_y < \mu_0 H^*_y$, $\varepsilon_\perp$ can be approximated as $\varepsilon_\perp \cong 1 - \psi^2_{eq}/2$, yielding

$$\varepsilon_\perp \cong 1 - \frac{1}{2}\left(\frac{\mu_0 H_y}{\mu_0 H_{DMI} - \mu_0 H_S}\right)^2. \quad (3)$$

This result implies that, when an in-plane magnetic field is applied perpendicular to the DW plane, the curvature β of $\varepsilon_\perp$ versus $\mu_0 H_y$ satisfies $\beta \equiv 1/[2(\mu_0 H_{DMI} - \mu_0 H_S)^2]$. Fig. 4(a) presents the variation of $\varepsilon_\perp$ as a function of $\mu_0 H_y$, where $\varepsilon_\perp = \cos\psi_{eq}$. The material parameters employed in the analysis were σ_0 = 10 mJ/m^2, $\mu_0 H_S$ = 30 mT, λ = 5 nm, M_S = 1 MA/m, and $\mu_0 H_{DMI}$ = 200 mT. Similar to the analysis in Fig. 2, $\varepsilon_\perp$ exhibits a clear quadratic dependence on $\mu_0 H_y$ for fields weaker than $\mu_0 H_y < \mu_0 H^*_y$. The purple solid line represents the calculated values obtained from Eq. (3), demonstrating excellent agreement within this low-field regime, where Eq. (3) remains valid.

When $\mu_0 H_{DMI} \gg \mu_0 H_S$ (i.e. materials with large DMI), the DMI-induced effective field can be estimated as $1/\sqrt{2\beta}$. Fig. 4(b) illustrates $1/\sqrt{2\beta}$ as a function of $\mu_0 H_{DMI}$ for each $\mu_0 H_S$. As discussed above, when $\mu_0 H_{DMI}$ dominates $\mu_0 H_S$, $1/\sqrt{2\beta}$ converges to $\mu_0 H_{DMI}$. This result indicates that large DMI values can be precisely quantified even under weak external magnetic fields by analyzing $\varepsilon_\perp(\mu_0 H_y)$ measured with in-plane fields perpendicular to the DW. Conversely, when $\mu_0 H_{DMI}$ is relatively small, it can be determined using conventional measurements of $\varepsilon_\perp$ as a function of the in-plane magnetic field applied along the x-axis $\mu_0 H_x$ [23-27]. Notably, large DMI values stabilize Néel-type DWs even in the absence of an in-plane magnetic field $\mu_0 H_y$. Under such conditions, the spin Hall angle can be independently extracted from measurements of SOT efficiency with respect to $\mu_0 H_y$. Accordingly, the proposed method provides a unified

framework for simultaneously evaluating the DMI and spin Hall angle across a broad range of magnitudes using field geometries optimized for each regime.

Various approaches have been proposed to quantify the DMI, including spin-wave spectroscopy [17-19], asymmetric DW motion [12], domain-edge tilting [14,20], asymmetric hysteresis-loop analysis [23-25], and SOT-efficiency measurements based on DW chiral transitions [26,27]. Among these, methods relying on spin waves, domain-edge tilting, or asymmetric DW motion are designed to isolate the DMI contribution alone, whereas the latter allow simultaneous determination of both SOT and DMI. However, the applicability of these conventional methods is typically limited to regimes where the in-plane magnetic field is significantly larger than the DMI-induced effective field. By contrast, the proposed approach enables the concurrent evaluation of SOT and DMI even when the in-plane field is significantly smaller than the DMI-induced effective magnetic field, thereby overcoming the constraints of existing techniques and offering broad utility for advancing chiral spintronics research.

III. Conclusion

In summary, the proposed framework establishes a simple yet robust route to quantify the DMI under experimentally accessible magnetic fields. By exploiting the quadratic response of DW magnetization to in-plane fields, the method directly links measurable curvature to the DMI and DW anisotropy energies. This approach enables the precise determination of large DMI strengths without relying on high-field measurements, thereby providing a broadly applicable tool for exploring chiral spin textures and their field-driven dynamics in a wide range of magnetic heterostructures.

Acknowledgements

We would like to thank Editage (www.editage.co.kr) for English language editing. This work was supported by the Korea Institute of Science and Technology (KIST) institutional program (grant 2E33581), and by the National Research Council of Science & Technology (NST) grant by the Korea government (MSIT) (No. GTL24041-000).

Author Contributions

D.H.K. conceived the idea and supervised the research. M.K. and D.H.K. developed the theoretical framework and analyzed the data. The manuscript was written by M.K. and D.H.K. All authors participated in discussions of the results and reviewed of the manuscript.

Additional information

Correspondence and requests for materials should be addressed to D.H.K.

Competing financial interests

The authors declare no competing financial interests.

Data availability

All data are available in the main text.

References

[1] I. E. Dzialoshinskii, Sov. Phys. JETP **5**, 1259 (1957).
[2] T. Moriya, Phys. Rev. **120**, 91 (1960).
[3] A. Fert and P. M. Levy, Phys. Rev. Lett. **44**, 1538 (1980).
[4] A. Fert, Mater. Sci. Forum **59-60**, 439 (1990).
[5] M. Bode, M. Heide, K. von Bergmann, P. Ferriani, S. Heinze, G. Bihlmayer, A. Kubetzka, O. Pietzsch, S. Blügel, and R. Wiesendanger, Nature **447**, 190 (2007).
[6] X. Z. Yu, Y. Onose, N. Kanazawa, J. H. Park, J. H. Han, Y. Matsui, N. Nagaosa, and Y. Tokura, Nature **465**, 901 (2010).
[7] A. Manchon, H. C. Koo, J. Nitta, S. M. Frolov, and R. A. Duine, Nat. Mater. **14**, 871 (2015).
[8] G. Bihlmayer, P. Noël, D. V. Vyalikh, E. V. Chulkov, and A. Manchon, Nat. Rev. Phys. **4**, 642 (2022).
[9] K.-S. Ryu, L. Thomas, S.-H. Yang, and S. Parkin, Nat. Nanotechnol. **8**, 527 (2013).
[10] O. Boulle, J. Vogel, H. Yang, S. Pizzini, D. d. S. Chaves, A. Locatelli, T. O. Menteş, A. Sala, L. D. Buda-Prejbeanu, O. Klein, M. Belmeguenai, Y. Roussigné, A. Stashkevich, S. M. Chérif, L. Aballe, M. Foerster, M. Chshiev, S. Auffret, I. M. Miron, and G. Gaudin, Nat. Nanotechnol. **11**, 449 (2016).
[11] K.-W. Moon, D.-H. Kim, S.-C. Yoo, S.-G. Je, B. S. Chun, W. Kim, B.-C. Min, C. Hwang, and S.-B. Choe, Sci. Rep. **5**, 9166 (2015).
[12] S.-G. Je, D.-H. Kim, S.-C. Yoo, B.-C. Min, K.-J. Lee, and S.-B. Choe, Phys. Rev. B **88**, 214401 (2013).
[13] J.-H. Moon, S.-M. Seo, K.-J. Lee, K.-W. Kim, J. Ryu, H.-W. Lee, R. D. McMichael, and M. D. Stiles, Phys. Rev. B **88**, 184404 (2013).
[14] S. Pizzini, J. Vogel, S. Rohart, L.D. Buda-Prejbeanu, E. Jué, O. Boulle, I. M. Miron, C. K. Safeer, S. Auffret, G. Gaudin, and A. Thiaville, Phys. Rev. Lett. **113**, 047203 (2014).
[15] V. E. Dmitrienko, E. N. Ovchinnikova, S. P. Collins, G. Nisbet, G. Beutier, Y. O. Kvashnin, V. V. Mazurenko, A. I. Lichtenstein, and M. I. Katsnelson, Nature Phys. **10**, 202 (2014).
[16] A. Hrabec, N. A. Porter, A. Wells, M. J. Benitez, G. Bur-

nell, S. McVitie, D. McGrouther, T. A. Moore, and C. H. Marrows, Phys. Rev. B **90**, 020402(R) (2014).
[17] M. Belmeguenai, *et al*., Phys. Rev. B **91**, 180405(R) (2015).
[18] J. Cho, N.-H. Kim, S. Lee, J.-S. Kim, R. Lavrijsen, A. Solignac, Y. Yin, D.-S. Han, N. J. J. van Hoof, H. J. M. Swagten, B. Koopmans, and C.-Y. You, Nat. Commun. **6**, 7635 (2015).
[19] H. T. Nembach, J. M. Shaw, M. Weiler, E. Jué, and T. J. Silva, Nature Phys. **11**, 825 (2015).
[20] D.-S. Han, N.-H. Kim, J.-S. Kim, Y. Yin, J.-W. Koo, J. Cho, S. Lee, M. Kläui, H. J. M. Swagten, B. Koopmans, and C.-Y. You, Nano Lett. **16**, 4438 (2016).
[21] J.-M. Lee, C. Jang, B.-C. Min, K.-J. Lee, and J. Chang, Nano Lett. **16**, 62 (2016).
[22] D.-H. Kim, D.-Y. Kim, S.-C. Yoo, B.-C. Min, and S.-B. Choe, Phys. Rev. B **99**, 134401 (2019).
[23] C.-F. Pai, M. Mann, A. J. Tan, and G. S. D. Beach, Phys. Rev. B **93**, 144409 (2016).
[24] T. Dohi, S. Fukami, and H. Ohno, Phys. Rev. B **103**, 214450 (2021).
[25] M. Kim and D.-H. Kim, Phys. Rev. B **112**, 024414 (2025).
[26] P. P. J. Haazen, E. Murè, J. H. Franken, R. Lavrijsen, H. J. M. Swagten, and B. Koopmans, Nat. Mater. **12**, 299 (2013).
[27] S. Emori, E. Martinez, K.-J. Lee, H.-W. Lee, U. Bauer, S.-M. Ahn, P. Agrawal, D. C. Bono, and G. S. D. Beach, Phys. Rev. B **90**, 184427 (2014).
[28] D.-H. Kim, S.-C. Yoo, D.-Y. Kim, B.-C. Min, and S.-B. Choe, Sci. Rep. **7**, 45498 (2017)
[29] D.-H. Kim, M. Haruta, H.-W. Ko, G. Go, H.-J. Park, T. Nishimura, D.-Y. Kim, T. Okuno, Y. Hirata, Y. Futakawa, H. Yoshikawa, W. Ham, S. Kim, H. Kurata, A. Tsukamoto, Y. Shiota, T. Moriyama, S.-B. Choe, K.-J. Lee, and T. Ono, Nat. Mater. **18**, 685 (2019).
[30] A. Thiaville, S. Rohart, É. Jué, V. Cros, and A. Fert, Europhys. Lett. **100**, 57002 (2012).
[31] R. O'Handley, Modern Magnetic Materials: Principles and Applications, Wiley-Interscience, New York (2000) pp. 274-312.